



## Phase diagram and thermoelastic property of iron oxyhydroxide across the spin crossover under extreme conditions

Bo Gan (甘波)<sup>1,2</sup> Gang Jiang (蒋刚)<sup>1</sup> Yuqian Huang (黄钰倩)<sup>1</sup> Hong Zhang (张红)<sup>3</sup> Qingyang Hu (胡清扬)<sup>4,\*</sup> and Youjun Zhang (张友君)<sup>1,5,†</sup>

<sup>1</sup>*Institute of Atomic and Molecular Physics, Sichuan University, Chengdu 610065, China*

<sup>2</sup>*Institute for Integrated Radiation and Nuclear Science, Kyoto University, Kumatori, Osaka 590-0494, Japan*

<sup>3</sup>*College of Physics, Sichuan University, Chengdu 610065, China*

<sup>4</sup>*Center for High Pressure Science and Technology Advanced Research, Beijing 100094, China*

<sup>5</sup>*International Center for Planetary Science, College of Earth Sciences, Chengdu University of Technology, Chengdu 610059, China*



(Received 31 August 2022; revised 5 February 2023; accepted 10 February 2023; published 28 February 2023)

Spin transition and its effect on the physical properties of iron-bearing minerals at high pressure-temperature ( $P$ - $T$ ) are of great importance for understanding the structural heterogeneity of Earth's mantle. Here, we investigate the phase diagram and thermoelastic properties of iron oxyhydroxide (FeOOH) across the spin crossover using dynamic high  $P$ - $T$  experiments and theoretical simulations. The Hugoniot equation of state in FeOOH has been measured up to  $\sim 90$  GPa and  $\sim 2100$  K in a two-stage light-gas gun and exhibits a density discontinuity between 47 GPa ( $\sim 950$  K) and 61 GPa ( $\sim 1150$  K) due to the high-low spin transition of  $\text{Fe}^{3+}$ , which is consistent with our first-principles calculations. The  $P$ - $T$  phase diagram indicates that the shock-elevated temperature shifts the spin transition to a higher pressure and broadens the pressure range of mixed spins. The large volume collapse of FeOOH during its spin crossover leads to remarkable elastic anomalies, with  $\sim 60\%$  softening of adiabatic bulk modulus and a negative Poisson's ratio ( $-0.1$ ) of abnormal auxeticity in the mixed-spin phase. Our results suggest that FeOOH undergoes an unselective spin transition of ferric iron at the corresponding  $P$ - $T$  conditions of the Earth's 1400–1800 km depth and exhibits drastic softening in sound velocities and elastic modulus which may be detected as seismic heterogeneities in subducting slabs of the lower mantle.

DOI: [10.1103/PhysRevB.107.064106](https://doi.org/10.1103/PhysRevB.107.064106)

### I. INTRODUCTION

Iron (Fe) is the most abundant transition-metal element in Earth's mantle [1,2]. Its incorporation and imposed effects on the physical properties of the lower-mantle minerals at high  $P$ - $T$  conditions are essential for understanding the evolution and structure of the Earth's mantle. Pressure-induced high-spin (HS) to low-spin (LS) transitions in iron-bearing lower-mantle minerals have been extensively studied using *in situ* synchrotron Mössbauer spectroscopy (SMS) [3], x-ray diffraction (XRD) [4,5], x-ray emission spectroscopy [6,7], and theoretical calculations [8,9]. Those pioneering works show that the spin transition of iron is usually accompanied by a volume collapse and remarkable changes in the geophysical and geochemical properties of the host mineral [10–18], which may further affect the dynamics and physicochemical state of Earth's lower mantle [1].

The valence state of an iron cation can be  $\text{Fe}^{2+}$  and/or  $\text{Fe}^{3+}$  in major mantle minerals, such as ferropierclase [(Mg,  $\text{Fe}^{2+}$ )O] and bridgmanite [(Mg,  $\text{Fe}^{3+}$ , Al)(Si,  $\text{Fe}^{3+}$ , Al) $\text{O}_3$ ]. The spin transition of ferrous ions in ferropierclase occurs in the  $\sim 35$ – $60$  GPa range at room and high temperatures, where the HS and LS states coexist in a wide pressure range [4,7,19,20]. The situation of  $\text{Fe}^{3+}$ -bearing

bridgmanite is more complex due to its crystal chemistry and the possibility of the intracrystalline partitioning of iron [3,21–23]. In short, our understanding of the spin transition of  $\text{Fe}^{3+}$  in the lower mantle has been hampered by the lack of high  $P$ - $T$  experimental data for  $\text{Fe}^{3+}$ -bearing phases.

Ferric oxyhydroxide ( $\text{Fe}^{3+}\text{OOH}$ ) is abundant and widespread on Earth's surface as mineral goethite ( $\alpha$ -FeOOH, space group  $Pbnm$ ,  $Z = 4$ ). Recent experiments and calculations show that goethite's high-pressure polymorph  $\epsilon$ -FeOOH (space group  $P2_1nm$ ,  $Pnmm$ ,  $Z = 2$ ) may carry water and/or hydrogen into the deep lower mantle and thus be an important  $\text{Fe}^{3+}$ -bearing and water-bearing phase in Earth's mantle [24–30]. Meanwhile, the spin state of  $\text{Fe}^{3+}$  in FeOOH has attracted intensive interest. Density functional theory (DFT) calculations predicted that the HS to LS transitions of  $\text{Fe}^{3+}$  in  $\alpha$ - and  $\epsilon$ -FeOOH phases would take place at  $\sim 60$  GPa [13,31–33]. However, single-crystal XRD, SMS, Raman spectroscopy, x-ray absorption spectroscopy, and resistivity measurements in a diamond anvil cell (DAC) at room temperature manifested that those spin transitions occurred at  $\sim 45$  GPa with a small mixed-spin (MS) interval of  $\sim 2$  GPa [5,13,31,34]. Several spin transition-induced anomalies in the physical properties of FeOOH were observed in these DAC experiments, such as a sudden volume collapse of  $\sim 11\%$  [5,13], a sharp decrease of the resistance by five orders of magnitude [31], and altered optical properties [5].

The effects of temperature on the spin transition of  $\text{Fe}^{3+}$  in  $\epsilon$ -FeOOH are relatively less investigated. The longitudinal

\*qingyang.hu@hpstar.ac.cn

†zhangyoujun@scu.edu.cn

sound velocity ( $V_p$ ) measurements under shock compression exhibited an abnormal softening of  $\sim 20\%$  between 46 and 60 GPa [12]. This pressure range is substantially wider than that observed in static compression experiments at room temperature [5,13], signifying the role of high temperature. Therefore, to understand the density and elastic properties of  $\varepsilon$ -FeOOH, it is urgent to conduct *in situ* experiments and simulations at the  $P$ - $T$  conditions relevant to Earth's lower mantle.

Here, we report the equation of state, thermoelastic property, and phase diagram of FeOOH across its spin crossover up to  $\sim 90$  GPa and  $\sim 2100$  K by shock compression experiments and first-principles calculations. The present results indicate that the spin transition of  $\text{Fe}^{3+}$  in  $\varepsilon$ -FeOOH starts at 47 GPa ( $\sim 950$  K) and completes at 61 GPa ( $\sim 1150$  K) along the Hugoniot, resulting in significant softening in bulk sound velocity ( $V_B$ ), adiabatic bulk modulus ( $K_S$ ), and Poisson's ratio ( $\nu$ ), while there is slight stiffening of shear sound velocity ( $V_S$ ) and shear modulus ( $\mu$ ). In this paper, we provide insight into the understanding of the spin-transition behavior and spin-transition-induced physical properties of  $\text{Fe}^{3+}$ - and/or water-bearing phases under high  $P$ - $T$  conditions of the lower mantle.

## II. METHODS

### A. Hugoniot data measurements in a two-stage light-gas gun

Natural goethite is a starting material that has been used in previous shock experiments [12]. The morphology and chemical composition of the used samples have been analyzed using XRD, an electron probe microanalyzer, and scanning electron microscopy, which can be found elsewhere [24]. The sample characterization shows that it is homogeneous and mainly composed of  $\alpha$ -FeOOH ( $\sim 95$  wt. %), minor amounts of quartz ( $\text{SiO}_2$ ,  $\sim 3$  wt. %) impurities, and few microvoids with  $\sim 2$   $\mu\text{m}$  in diameter. We measured the initial density of each sample ( $\sim 12$  mm diameter,  $\sim 2$  mm thick) using the Archimedeian method. It ranged between  $3.901$  and  $3.920$   $\text{g}/\text{cm}^3$  and was  $\sim 8\%$  lower than the ideal density of  $4.25$   $\text{g}/\text{cm}^3$  due to impurities and little porosity in the natural sample [24]. The sample was polished on both parallel surfaces to ensure precise shock velocity measurements.

Planar impact experiments were conducted using a two-stage light-gas gun with a 25 mm bore tube at the Institute of Atomic and Molecular Physics, Sichuan University. We measured the impact velocity of the flyer ( $w$ ) and shock wave velocity in the sample ( $U_S$ ) to determine the Hugoniot states. Here, the values of the impact velocity and shock wave velocity of the sample were measured by an electromagnetic method and an electrical pin technique, respectively (Text S1 in the Supplemental Material [35]). Copper (Cu) and Fe were used as flyer and base plates. After obtaining the shock wave velocity of the FeOOH, the particle velocity ( $u_p$ ) was calculated using the impedance matching method based on the impact velocity and the known Hugoniot relations of Cu [36,37] and Fe [38] (Fig. S3 in the Supplemental Material [35]). Eleven forward impact experiments were performed, and the impact velocity ranged from 2.14 to 4.62 km/s (Table I). The Hugoniot data of FeOOH were obtained in the

pressure range of 35.2–88.4 GPa. We also analyzed the impact velocity and particle velocity at the FeOOH/lithium fluoride (LiF) interface measured in the previous reverse-impact experiments [12] to obtain the Hugoniot data of FeOOH at lower pressures of 25.3–31.5 GPa (Table I). We estimated the uncertainties of the measured Hugoniot data based on the analysis of error propagation [36], which are generally  $< \sim 2\%$ .

### B. First-principles simulation for the spin crossover and equation of state

The spin fraction parameter  $n_{LS}$  of  $\varepsilon$ -FeOOH was investigated under high  $P$ - $T$  conditions using first-principles simulation. We first calculated the free energies of  $\varepsilon$ -FeOOH at both HS and LS states, whose vibrational energies were approximated by the quasiharmonic model. The calculation was performed under the framework of DFT through the Vienna *Ab initio* Simulation Package (ver. 5.4.4) [40], in which we used the plane-wave augmented pseudopotentials. The configurations of valence electrons for each atom species were Fe,  $3d^7 4s^1$ ; O,  $2s^2 2p^4$ ; and H,  $1s^1$ . The electron-correlation energies were parameterized by Perdew, Burke, and Ernzerhof [41]. We set the cutoff energy of plane-wave basis as 800 eV. The Brillouin zone was sampled such that the smallest allowed spacing between  $k$  points was  $0.2 \text{ \AA}^{-1}$ . We tested the convergence of results by varying the kinetic energy cutoff, and we are convinced our setup can produce robust results (Table SI in the Supplemental Material [35]). The geometric optimization at each pressure was achieved by converging forces to  $0.005 \text{ eV}/\text{Å}$  on each atom. To describe the strongly correlated system, we employed a fixed Hubbard term  $U - J = 5.3$  eV, with  $J = 1.36$  eV, which has previously described the spin transition of  $\text{Fe}^{3+}$  in  $\varepsilon$ -FeOOH [13] and was set according to the calculated atomic Slater integrals for ferric iron.

The thermodynamics during the spin transition of  $\text{Fe}^{3+}$  in  $\varepsilon$ -FeOOH is treated as an ideal solid solution of the HS and LS phases. This approximation has been used to successfully describe the MS state of ferropicriase [42] and the elastic wave softening of  $\varepsilon$ -FeOOH at the MS state [12]. These relations are

$$V(n_{LS}, P, T) = n_{LS}V_{LS}(P, T) + (1 - n_{LS})V_{HS}(P, T), \quad (1)$$

$$\frac{V(n_{LS})}{K(n_{LS})} = n_{LS} \frac{V_{LS}}{K_{LS}} + (1 - n_{LS}) \frac{V_{HS}}{K_{HS}} - (V_{LS} - V_{HS}) \left. \frac{\partial n_{LS}}{\partial P} \right|_T, \quad (2)$$

where  $n_{LS}$  is the fraction of the LS state, and  $V_{LS}$ ,  $V_{HS}$ ,  $K_{LS}$ , and  $K_{HS}$  are the equilibrium volume and isothermal compressibility of pure LS and HS states, respectively. The above equations are the same ones used in Ref. [42], and the properties of the MS  $\varepsilon$ -FeOOH can be determined from those of the LS and HS states and the fraction of the LS state, all of which were computed individually.

The validity territory of using the quasiharmonic approximation is defined by the trend of its thermal expansivity (Fig. S4 in the Supplemental Material [35]). We shall note that the asymmetric hydrogen bond is well known to produce the double welling on the free energy surface and create

TABLE I. Impact conditions and Hugoniot results for the FeOOH<sup>a</sup>.

Shot No.	Sample		Flyer/base plate	$w$ (km/s)	$U_{\text{int}}$ (km/s)	$P_{\text{H}}$ (GPa)	$T_{\text{est.}}$ (K)	$u_{\text{p}}$ (km/s)	$U_{\text{S}}$ (km/s)	$\rho_{\text{H}}$ (g/cm <sup>3</sup> )
	$\rho_0$ (g/cm <sup>3</sup> )	$d$ (mm)								
Forward impact										
F1	3.919(5)	2.028(6)		2.142(10)		35.2(0.5)	680(102)	1.366(21)	6.569(89)	4.948(67)
F2	3.902(5)	2.040(6)		2.241(11)		36.8(0.9)	715(107)	1.437(35)	6.561(155)	4.996(118)
F3	3.906(5)	2.096(6)		2.392(12)		40.2(0.7)	790(119)	1.529(29)	6.722(120)	5.056(90)
F4	3.911(5)	2.041(6)		2.672(13)		46.3(0.2)	930(140)	1.705(15)	6.947(33)	5.183(25)
F5	3.902(5)	2.030(6)		2.799(14)		48.4(0.4)	967(145)	1.797(20)	6.907(58)	5.274(44)
F6	3.901(5)	2.005(6)	Cu/Cu	2.962(15)	—	51.4(0.4)	1007(151)	1.912(21)	6.897(56)	5.397(44)
F7	3.903(5)	1.941(5)		3.213(16)		56.2(0.8)	1072(161)	2.089(32)	6.898(95)	5.598(77)
F8	3.921(5)	2.045(6)		3.509(18)		62.5(0.9)	1182(177)	2.291(37)	6.958(101)	5.846(85)
F9	3.901(5)	1.962(5)		3.542(18)		62.9(0.9)	1197(180)	2.317(35)	6.959(94)	5.848(79)
F10	3.920(5)	2.054(6)		3.822(19)		70.3(1.4)	1432(215)	2.492(52)	7.192(140)	5.998(117)
F11	3.901(5)	2.089(6)	Fe/Fe	4.621(23)		88.4(1.0)	2069(310)	2.920(38)	7.763(84)	6.252(68)
Reverse impact										
R1	3.935(5)	2.024(6)	Goethite/—	2.432(12)	1.361(22)	25.3(0.8)	510(77)	1.071(25)	6.014(188)	4.787(124)
R2	3.921(5)	2.024(6)		2.879(14)	1.615(38)	31.5(1.3)	615(92)	1.264(40)	6.363(248)	4.895(154)

<sup>a</sup>Note:  $\rho_0$  and  $d$  are the initial density and thickness of our samples, respectively;  $w$  is the measured impact velocity of the flyer;  $U_{\text{int}}$  is the measured particle velocity at the sample/LiF interface in the reverse impact experiments [12];  $P_{\text{H}}$  is the Hugoniot pressure, which is calculated using the impedance matching method;  $T_{\text{est.}}$  is the estimated Hugoniot temperature, which is calculated by a thermodynamic equation;  $u_{\text{p}}$  and  $U_{\text{S}}$  are the particle velocity and shock velocity in the shocked sample, respectively;  $\rho_{\text{H}}$  is the density at Hugoniot state. In the forward impact experiments, the flyer plate and base plate are of the same material, where Cu and Fe were used in shots No. F1–F10 and shot No. F11, respectively. In the reverse impact experiments, the goethite sample was used as the flyer to directly impact the LiF window. The experimental data of the forward impact (shots No. F1–F11,  $P_{\text{H}} > 35$  GPa) and reverse impact (shots No. R1–R2,  $P_{\text{H}} < 35$  GPa) are obtained in this paper and from the previous study [12], respectively. The Hugoniot parameters used in this paper are  $U_{\text{S}}$  (km/s) = 5.215(0.02) + 1.351(0.03) $u_{\text{p}}$  with the initial density of 2.640 (0.002) g/cm<sup>3</sup> for LiF [39],  $U_{\text{S}}$  (km/s) = 3.933(0.004) + 1.500(0.025) $u_{\text{p}}$  with the initial density of 8.939 (0.005) g/cm<sup>3</sup> for Cu [36,37],  $U_{\text{S}}$  (km/s) = 3.94(0.02) + 1.58(0.01) $u_{\text{p}}$  with the initial density of 7.85 (0.03) g/cm<sup>3</sup> for Fe [38]. Values in parentheses reflect uncertainties, which are given in parameters at  $2\sigma$  level.

dynamic instability (Fig. S5 in the Supplemental Material [35]) [43,44]. From our phonon spectroscopy, the structure starts to be mechanically stable at  $>40$  GPa. Since the spin-transition boundary starts at  $\sim 45$  GPa, our treatment of the calculation should be valid at the sensitive pressure regime of this paper.

Here, the fraction  $n_{\text{LS}} = n_{\text{LS}}(P, T)$  is obtained by minimizing the Gibbs free energy ( $G$ ) with respect to  $n_{\text{LS}}$  by following the formula:

$$n_{\text{LS}}(P, T) = \frac{1}{1 + m(2S + 1) \exp\left[\frac{\Delta G_{\text{LS-HS}}}{k_{\text{B}}T}\right]}, \quad (3)$$

where  $S$  and  $m$  are the total spin quantum number and electronic configuration degeneracy, respectively, and  $\Delta G_{\text{LS-HS}}$  is the difference between the free energy of the LS and HS states. This equation includes both static and vibrational contributions at different  $P$  and  $T$ . We approximated the vibrational energy by the integrals of phonons according to the quasi-harmonic approximation, and it was performed by PHONOPY 2.4.2 [45]. Details of the methodology are also found in Ref. [46].

The pressure ( $P$ ), volume ( $V$ ), and internal energy ( $E$ ) across a shock front can be determined based on the Rankine-Hugoniot equation given as [36]

$$\frac{1}{2}(P_{\text{H}} + P_0)(V_0 - V_{\text{H}}) = E_{\text{H}} - E_0, \quad (4)$$

where subscripts H and 0 denote the states at Hugoniot pressure and the ambient conditions, respectively. The  $P$ - $V$  and  $P$ - $T$  relations on the Hugoniot are then determined by first-principles molecular dynamics (FPMD) simulation. The kinetic energy cutoff was the same as structural optimization but only a  $\gamma$ -center  $k$  point was used for FPMD simulation. To fix spin, we assumed a paramagnetic configuration for the LS state and a ferromagnetic configuration for the HS state (fixed at  $4.0 \mu_{\text{B}}$ ). This strategy has been used for similar iron-bearing systems [47], and we found this is probably the only way to produce robust energies on fixed volume and temperature without too much perturbation of magnetization. In comparison, if we initialize an antiferromagnetic state, the trajectory will feature the mixed LS, medium-spin, and HS states of iron. The system for MD simulation consists of 64 atoms ( $2 \times 2 \times 2$  supercell, 16 Fe, 32 O, and 16 H). An NVT molecular dynamics simulation was run for each  $P$ - $T$  point for 2000 timesteps, and the last 1000 steps of each were taken for calculating energy and pressure. For a given  $V_{\text{H}}$ , the principal Hugoniot state was determined by interpolation of a series of equilibrium calculations at different temperatures so that Eq. (4) was satisfied [48–51]. Based on the experimental measurements [5], the HS and LS volumes of FeOOH at the initial pressure ( $P_0 = 0$ ) are  $V_{0, \text{HS}} = 0.225 \text{ cm}^3/\text{g}$  and  $V_{0, \text{LS}} = 0.192 \text{ cm}^3/\text{g}$ , respectively. The initial internal energies of FeOOH at the HS and LS states are  $E_{0, \text{HS}} = -25.551 \text{ eV/fu}$  and  $E_{0, \text{LS}} = -25.811 \text{ eV/fu}$ , respectively, at a temperature of 300 K.

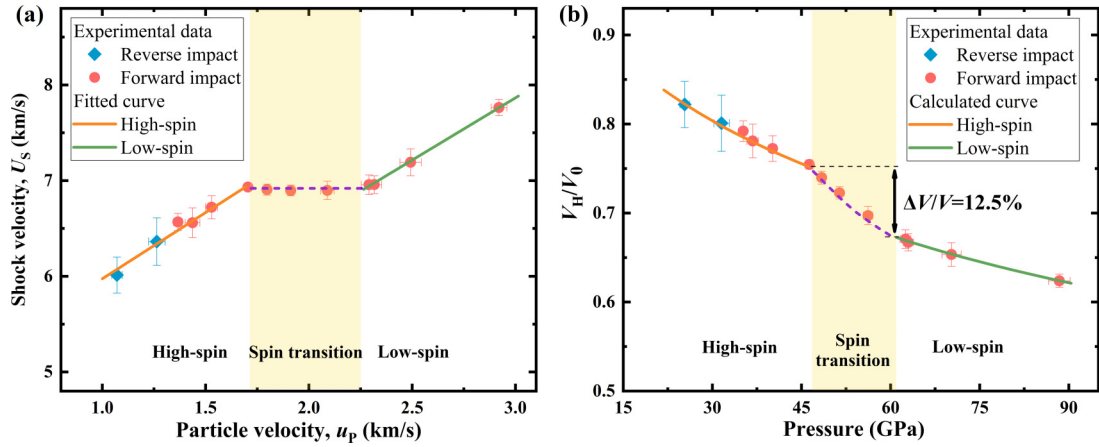


FIG. 1. Hugoniot equation of state for the natural goethite under shock compression. (a) The relation between the shock velocity and particle velocity ( $U_s - u_p$ ). (b) The relation between the Hugoniot pressure and specific volume ( $P$ - $V$ ). The red circles and blue diamonds are experimental data determined by forward and reverse impacts in this paper and reanalyzed from the previous data [12], respectively; the orange and green lines are fitted (or calculated) results for the high- and low-spin states, respectively; the light-shaded area represents the spin crossover region with the mixed-spin state; the dashed violet line is to guide the eye.

### III. RESULTS AND DISCUSSION

#### A. Hugoniot equation of state of $\varepsilon$ -FeOOH under dynamic compression

A total of 13 sets of Hugoniot data were collected for FeOOH in the pressure range of 25.3–88.4 GPa, as shown in Table I and Fig. 1. It has been shown that  $\alpha$ -FeOOH undergoes a first-order phase transition to form the high-pressure  $\varepsilon$ -FeOOH phase at  $\sim 6$ –10 GPa [52–56]. The pressure range in this study is substantially larger than the phase boundary between  $\alpha$ -FeOOH and  $\varepsilon$ -FeOOH. Therefore, it is expected that the starting  $\alpha$ -FeOOH would transform into  $\varepsilon$ -FeOOH at  $\sim 6$ –10 GPa along the Hugoniot. Further shock compression experiments are required to measure the Hugoniot data and

sound velocity of FeOOH to accurately determine its  $\alpha$ - $\varepsilon$  phase transition along the Hugoniot. In Fig. 1, the shock wave velocity–particle velocity ( $U_s - u_p$ ) relation [pressure-specific volume ( $P$ - $V$ ) relation] shows significant changes around  $u_p = 1.72$  km/s ( $P_H = 47$  GPa) and  $u_p = 2.25$  km/s ( $P_H = 61$  GPa). Based on recent theoretical and experimental studies [5,13], three different regimes, namely, HS behavior  $< 47$  GPa, LS behavior  $> 61$  GPa, and a spin crossover region between 47 and 61 GPa, were identified and in good agreement with the previous measurements of longitudinal sound velocity under shock compression [12]. The quasilinear correlations between shock wave velocity ( $U_s$ ) and particle velocity ( $u_p$ ) are shown as follows:

$$U_s = C_0 + \lambda u_p = \begin{cases} 4.49(\pm 0.16) + 1.46(\pm 0.10)u_p, & (u_p < 1.72, \text{ HS state}) \\ 6.92(\pm 0.12), & (1.72 \leq u_p \leq 2.25, \text{ MS state}) \\ 3.75(\pm 0.33) + 1.39(\pm 0.14)u_p, & (u_p > 2.25, \text{ LS state}), \end{cases} \quad (5)$$

where  $\lambda$  is a constant;  $U_s$ ,  $u_p$ , and  $C_0$  are in km/s; and values in parentheses are uncertainties, which are given at  $2\sigma$  level. Within the spin crossover region, the  $U_s$  remains almost constant with the increase of the  $u_p$ . This result indicates that the propagation of the shock wave in the shocked  $\varepsilon$ -FeOOH is hindered by the electronic spin crossover of  $\text{Fe}^{3+}$  because part of the energy carried by the shock wave is used for spin pairing. The  $U_s$  plateau with increasing  $u_p$  also appears in other iron oxides, such as  $\text{Fe}_2\text{O}_3$  [57], which undergoes a site-selective HS-to-LS transition at 46–50 GPa [58–61].

Based on the determined  $U_s$  and  $u_p$ , the density at the Hugoniot state ( $\rho_H$ ) can be calculated using the Rankine-Hugoniot conservation equations [36]:

$$\frac{V_0}{V_H} = \frac{\rho_H}{\rho_0} = \frac{U_s - u_0}{U_s - u_p}, \quad (6)$$

where  $V = 1/\rho$ . Our measured density under shock compression is slightly lower than the densities from XRD experiments (300 K) [5,13] and our DFT calculations by 2–7% and 0–3% (Fig. 2), respectively, which is most likely caused by the impurities and few porosities in the initial samples (Fig. S6 in the Supplemental Material [35]). We also obtained the pressure-density ( $P$ - $\rho$ ) Hugoniot relations of  $\varepsilon$ -FeOOH in the HS and LS states by the following formula:

$$P_H = \frac{\rho_0 C_0 \eta}{(1 - \lambda \eta)^2}, \quad (7)$$

where  $\eta = 1 - V_H/V_0$ . The Hugoniot relation shows a continuous volume reduction of the MS  $\varepsilon$ -FeOOH along the Hugoniot, and the volume was reduced by  $\sim 12.5\%$  across the spin crossover (47–61 GPa). The volume collapse across the electronic spin crossover varies in many iron-bearing phases, such as ferropericlase (1–4%) [1,9,42,62],  $\text{Fe}^{3+}$ -bearing

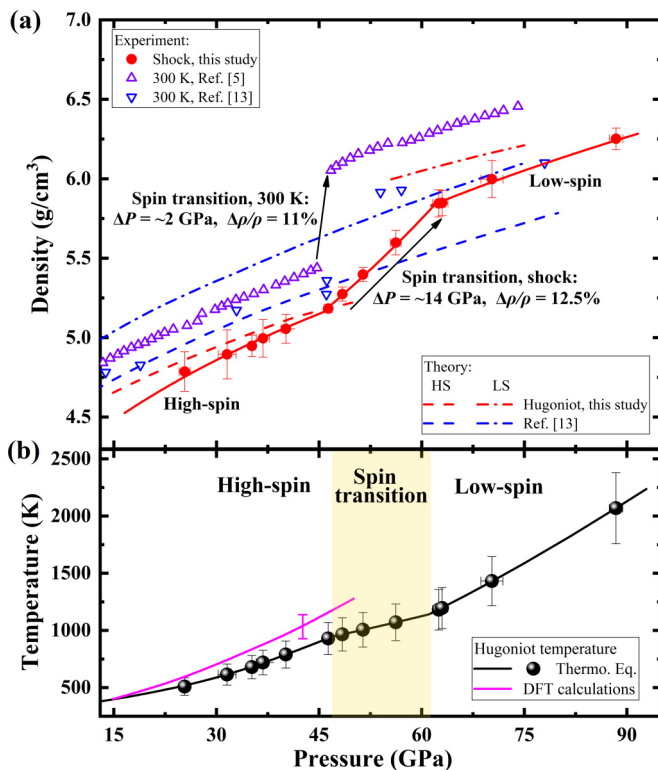


FIG. 2. Equation of state of FeOOH across the spin crossover at high pressure-temperature. (a) The density of FeOOH under static and shock compression. (b) Hugoniot temperature of FeOOH under shock compression. The solid red circles are Hugoniot density determined by using natural goethite in this paper; the open violet triangles [5] and blue inverted triangles [13] are densities determined by *in situ* x-ray diffraction (XRD) at high pressures and 300 K; the solid red line is the pressure-density ( $P$ - $\rho$ ) Hugoniot relation of the natural goethite; the red dashed and dotted dashed lines are Hugoniot densities of the high-spin (HS) and low-spin (LS) states from our density functional theory (DFT) calculations, respectively; the blue dashed and dotted dashed lines are isothermal pressure-density relations of the HS and LS states from DFT calculations by Ref. [13], respectively; the carmine line and solid black line (circles) are shock temperatures determined from our DFT calculations and the thermodynamic equation, respectively.

bridgmanite [22,63–65], magnesiosiderite [(Mg, Fe<sup>2+</sup>)CO<sub>3</sub>] (6–10%) [14,66–71], and the new hexagonal aluminous (NAL) phase (1%) [72]. The volume reduction of  $\epsilon$ -FeOOH is notably greater than those of the aforementioned phases, which verifies the strong dependence between the volume collapse and the iron content.

Static compression studies indicated that  $\epsilon$ -FeOOH undergoes a sharp spin transition of Fe<sup>3+</sup> by a large volume reduction of  $\sim 11\%$  within a narrow pressure interval of  $\sim 2$  GPa at room temperature (Fig. 2) [5,13]. Our shock experiments feature a higher onset pressure of the spin transition (47 GPa vs 45 GPa) and a broader pressure range of the spin crossover (14 GPa vs 2 GPa) than those results by DAC at room temperature. Previous studies have shown that shock wave measurements may broaden the pressure intervals of first-order phase transitions compared with static compression experiments due to the partial phase transition of the sample

within the time scale of the shock experiment [73–75]. The transformation rates of second-order phase transitions (e.g., electronic spin transitions) should be much faster than that of the first-order phase transitions [73,76]. Additionally, the  $V_p$  measurements under shock compression determine the velocity of the rarefaction wave in a shock-compressed sample, which is more sensitive to phase transitions than Hugoniot data measurements. Our determined pressure interval is in good agreement with the  $V_p$  results [12], indicating that it may not be broadened by the limited time interval during the shock. Therefore, this difference could be caused by the shock-elevated temperature in  $\epsilon$ -FeOOH, which has been found in other iron-bearing minerals, such as ferroperricite and bridgmanite [8,9,42,77–80]. The elevated temperature of the shocked  $\epsilon$ -FeOOH can be estimated based on the measured Hugoniot equation of state by using a thermodynamic equation [Table I and Fig. 2(b)] [81]:

$$dT = -T \left( \frac{\gamma}{V} \right) dV + \left( \frac{1}{2C_v} \right) [(V_0 - V)dP + (P - P_0)dV], \quad (8)$$

where  $\gamma$  and  $C_v$  are the Grüneisen parameter and specific heat capacity, respectively. The volume dependence of  $\gamma$  for the shocked FeOOH can be modeled by a common functional form as  $\gamma = \gamma_0(\rho_0/\rho)$ . Here,  $\gamma_0$  and  $C_v$  of  $\alpha$ -FeOOH were determined to be  $0.91 (\pm 0.07)$  [52] and  $0.837$  J/(K·g) [82], respectively. The uncertainty of the calculated shock temperature could be estimated from the uncertainties of the measured Hugoniot equation of state,  $\gamma$ , and  $C_v$  of FeOOH. If we consider a large uncertainty in the  $\gamma$  and  $C_v$  parameters (30–50%) under shock compression, it will change the shock temperature by 10–20% at the pressure range of 30–90 GPa. As a result, the calculated shock temperature of FeOOH has an overall uncertainty of 15% at the investigated shock pressure and is slightly lower than the temperature determined from our DFT calculations. The shock temperature in  $\epsilon$ -FeOOH increased from  $\sim 950$  to  $\sim 1150$  K between 47 and 61 GPa across its spin crossover. The temperature in  $\epsilon$ -FeOOH under single shock compression is much lower than that of shock recovery experiments [24]. Thus, the present results can be used to further constrain the phase boundary and decomposition of  $\epsilon$ -FeOOH at high  $P$ - $T$  (Text S2 and Fig. S7 in the Supplemental Material [35]).

### B. High $P$ - $T$ phase diagram of $\epsilon$ -FeOOH across the spin crossover of Fe<sup>3+</sup>

To further understand the effects of temperature on the spin-transition behavior of Fe<sup>3+</sup> in  $\epsilon$ -FeOOH, we constructed the high  $P$ - $T$  phase diagram of the spin state of Fe<sup>3+</sup> in  $\epsilon$ -FeOOH up to 75 GPa and 2000 K using first-principles calculations (Fig. 3). The phase diagram shows that the electronic spin-pairing transition of Fe<sup>3+</sup> in  $\epsilon$ -FeOOH starts at  $\sim 43$  GPa and completes at  $\sim 46$  GPa at 300 K, in good agreement with the results of static compression experiments at room temperature [5,13]. The crystal field theory shows that, at a constant temperature, the spin state of iron is determined by the energy difference between two energy levels of the crystal-field splitting energy ( $\Delta_C$ ) and the spin-pairing energy ( $\Delta$ ) [85]. It is energetically favorable for the spin pairing of

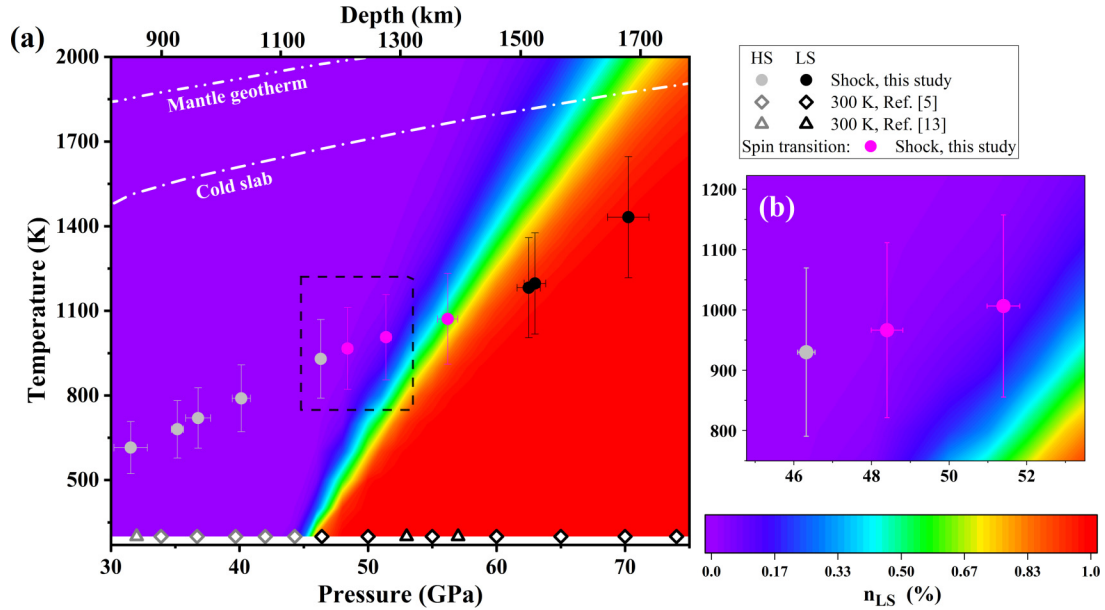


FIG. 3. Phase diagram of the spin crossover of  $\text{Fe}^{3+}$  in  $\varepsilon\text{-FeOOH}$  at high pressure-temperature. The gray circles (this paper), diamonds [5], and triangles [13] represent the high-spin state; the black circles (this paper), diamonds [5], and triangles [13] represent the low-spin (LS) state; the carmine circles are  $\varepsilon\text{-FeOOH}$  in the mixed-spin state observed by this paper. Colors in the horizontal column on the bottom right represent fractions of the LS  $\text{Fe}^{3+}$ ,  $n_{LS}$  (%), in  $\varepsilon\text{-FeOOH}$ . The area surrounded by the black dotted line in (a) is enlarged into (b), which shows that the onset of the spin transition of  $\text{Fe}^{3+}$  observed in our shock experiments is in good agreement with our first-principles calculations. The double dots and dotted dashed lines represent the proposed mantle [83] and subducting slab geotherms [84], respectively.

the  $3d$  electrons from the higher-energy  $e_g$  orbitals to the lower-energy  $t_{2g}$  orbitals once the crystal-field splitting energy is larger than the spin-pairing energy at high pressures [1]. Our theoretical results confirm that the crystal-field splitting energy increases with respect to the spin-pairing energy at 300 K as the pressure increases to  $\sim 43$  GPa.

In Fig. 3, it is obvious that the spin transition of  $\text{Fe}^{3+}$  in  $\varepsilon\text{-FeOOH}$  becomes slower under high temperatures, consistent with experiments. Our numerical analyses suggest that the onset and ending pressures of the spin transition of  $\text{Fe}^{3+}$  in  $\varepsilon\text{-FeOOH}$  increase at rates of  $\sim 8$  and  $\sim 18$  MPa/K, respectively, while the resultant pressure interval of the MS state broadens at a rate of  $\sim 10$  MPa/K. Such a positive correlation between spin-transition pressure and temperature has also been observed in  $\text{Fe}^{2+}$ -bearing phases. The temperature derivatives of the spin-transition pressure of ferroperricite and magnesiosiderite containing 25–65 mol.%  $\text{Fe}^{2+}$  are 12–14 MPa/K [8,66], which is 50–75% steeper than that of  $\varepsilon\text{-FeOOH}$ . We speculate that the spin-transition behavior of  $\text{Fe}^{2+}$ -bearing phases is more sensitive to variations in temperature than that of  $\text{Fe}^{3+}$ -bearing phases. At constant  $P$  and  $T$ , the difference between the free energy of the LS and HS states ( $\Delta G_{\text{LS-HS}}$ ) can be calculated by the following equation:

$$\Delta G_{\text{LS-HS}} = \Delta U_{\text{LS-HS}} - T \Delta S_{\text{LS-HS}} + P \Delta V_{\text{LS-HS}}, \quad (9)$$

where  $\Delta U_{\text{LS-HS}}$ ,  $\Delta S_{\text{LS-HS}}$ , and  $\Delta V_{\text{LS-HS}}$  represent the changes in internal energy, entropy, and volume across the spin crossover, respectively. It can be found that the contribution to the Gibbs free energy from the entropy term will become more substantial with increasing temperature, and consequently, the contribution of vibrational entropy ( $S_{\text{vib}}$ ) to the  $\Delta S_{\text{LS-HS}}$  is more viable [8,80]. Because of the occupation

of both  $e_g$  and  $t_{2g}$  orbitals, the HS iron ions are reported to feature a higher diffusion rate than the LS iron ions in the temperature range we investigated in this study [8]. Therefore, the vibrational entropy in the HS iron ions is greater than that of the LS iron ions [8,86]. With stronger vibrational, an increased amount of enthalpy is needed to overcome the increase of  $\Delta G_{\text{LS-HS}}$  through the entropy term [8,80]. Moreover, the magnetic term ( $S_{\text{mag}}$ ) is also an important component of the  $\Delta S_{\text{LS-HS}}$  [9] and can be expressed as follows [85]:

$$S_{\text{mag}} = k_B \ln [m(2S + 1)], \quad (10)$$

where  $k_B$  is the Boltzmann constant. Here,  $S_{\text{mag}}$  decreases from  $k_B \ln(15)$  to 0 across the HS-LS transition of  $\text{Fe}^{2+}$  ( $S = 2$  and  $m = 3$  for the HS  $\text{Fe}^{2+}$ ;  $S = 0$  and  $m = 1$  for the LS  $\text{Fe}^{2+}$ ). While,  $S_{\text{mag}}$  does not change across the HS-LS transition for  $\text{Fe}^{3+}$  and is equal to  $k_B \ln(6)$  ( $S = \frac{5}{2}$  and  $m = 1$  for the HS  $\text{Fe}^{3+}$ ;  $S = \frac{1}{2}$  and  $m = 3$  for the LS  $\text{Fe}^{3+}$ ). Therefore, due to the additional effect of the magnetic entropy, the onset pressure of the spin transition of ferrous ions in  $\text{Fe}^{2+}$ -bearing phases exhibits a larger temperature derivative than that of ferric ions in  $\text{Fe}^{3+}$ -bearing phases, even at lower content of iron ions.

In the spin crossover region, the configuration entropy ( $S_{\text{conf}}$ ) of the MS state is defined as follows [9]:

$$S_{\text{conf}} = -k_B [n_{\text{LS}} \ln n_{\text{LS}} + (1 - n_{\text{LS}}) \ln (1 - n_{\text{LS}})]. \quad (11)$$

A recent first-principles study indicates that the configuration entropy increased with the increase in temperature because of the relaxation of short-range order within the iron sites in the MS state [8]. Thus, increasing temperature favors the MS state due to the decrease of the free energy from the

$S_{\text{conf}}$  term, which explains the widening of the spin crossover pressure range of  $\text{Fe}^{3+}$  in  $\varepsilon$ -FeOOH with increasing temperature.

### C. Thermoelastic properties of $\varepsilon$ -FeOOH across the spin crossover of $\text{Fe}^{3+}$

In terms of the determined Hugoniot equation of state, the bulk sound velocity ( $V_B$ ) of  $\varepsilon$ -FeOOH in the HS and LS states can be calculated by the following equation along the Hugoniot pressure [Fig. 4(a)] [81]:

$$V_B^2 = -V_H^2 \frac{dP_H}{dV_H} \left[ 1 - \left( \frac{\gamma}{V_H} \right) \frac{(V_0 - V_H)}{2} \right] + V_H^2 \left( \frac{\gamma}{V_H} \right) \frac{P_H}{2}. \quad (12)$$

The estimated  $V_B$  in the spin crossover region shows a significant softening and is like the measured  $V_P$  under shock compression [12]. The uncertainty of the calculated  $V_B$  is  $\sim 2\%$  based on the measured Hugoniot equation of state and estimated  $\gamma$  at the pressure range of 20–70 GPa. According to the measured  $V_P$  and calculated  $V_B$ , the shear sound velocity  $V_S$  of  $\varepsilon$ -FeOOH along the Hugoniot pressure can be determined using the following relationship [Fig. 4(a)]:

$$V_S^2 = \frac{3}{4}(V_P^2 - V_B^2). \quad (13)$$

Extrapolating the derived  $V_S$  down to  $\sim 20$  GPa, the present result is consistent with the measured  $V_S$  using an ultrasonic pulse-echo-overlap method by Ref. [30]. Unlike the softening of  $V_P$  and  $V_B$  in the spin crossover region,  $V_S$  increases monotonically over the whole pressure range and stiffens slightly across the spin crossover of  $\text{Fe}^{3+}$ . We calculated the adiabatic bulk modulus  $K_S$  and shear modulus  $\mu$  of  $\varepsilon$ -FeOOH from its sound velocities ( $V_S$  and  $V_P$ ) along the Hugoniot pressure using the following equations [Fig. 4(b)] [88]:

$$K_S = \rho_H \left( V_P^2 - \frac{4}{3} V_S^2 \right), \quad (14)$$

$$\mu = \rho_H V_S^2. \quad (15)$$

The adiabatic bulk modulus of  $\varepsilon$ -FeOOH exhibits a remarkable softening by  $\sim 60\%$ , whereas the shear modulus stiffens slightly across the spin crossover of  $\text{Fe}^{3+}$ . Softening of adiabatic bulk modulus and stiffening of shear modulus have also been observed in Fe-bearing bridgmanite, ferroperricite, and magnesiosiderite [11,19,20,42,46,80,89,90]. Thus, our observed anomalous softening of the adiabatic bulk modulus and stiffening of the shear modulus can be attributed to the anomalous softening of elastic constants  $C_{11}$ ,  $C_{12}$ ,  $C_{13}$ ,  $C_{22}$ ,  $C_{23}$ , and  $C_{33}$ , and the stiffening of  $C_{44}$ ,  $C_{55}$ , and  $C_{66}$  of the MS  $\varepsilon$ -FeOOH, respectively (Text S3 in the Supplemental Material [35]).

Poisson's ratio ( $\nu$ ) describes the mechanical properties of minerals, which can be expressed in terms of sound velocities using the following equation [91]:

$$\nu = \frac{[(V_P/V_S)^2 - 2]}{2[(V_P/V_S)^2 - 1]}. \quad (16)$$

We calculate Poisson's ratio of  $\varepsilon$ -FeOOH along the Hugoniot pressure [Fig. 4(c)]. The result shows that Poisson's ratio of

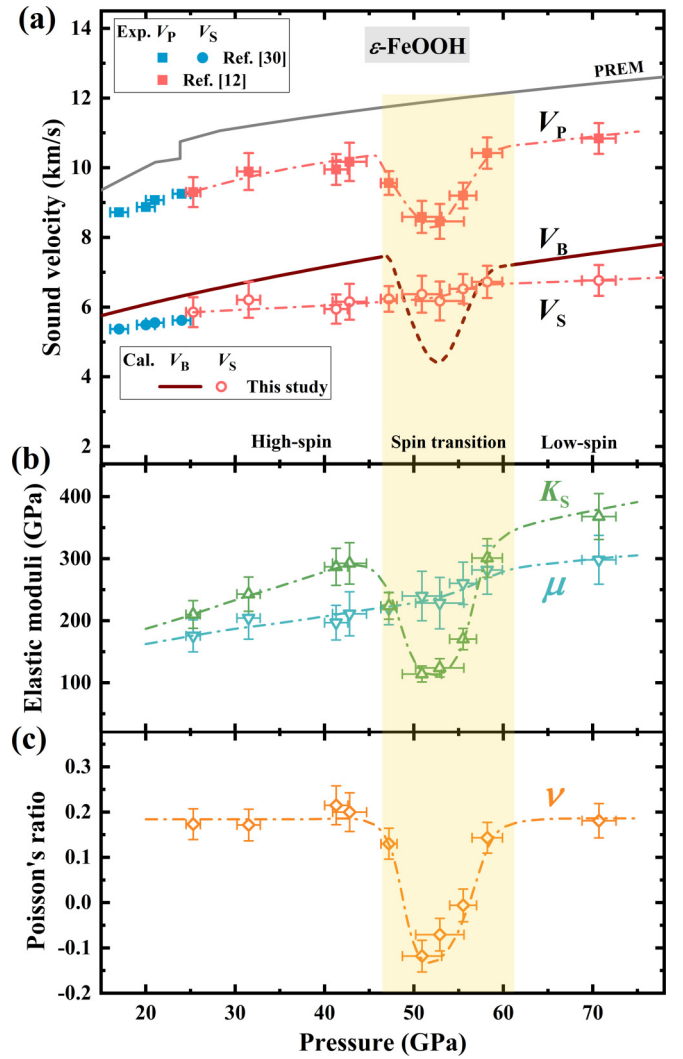


FIG. 4. (a) Sound velocities, (b) elastic parameters, and (c) Poisson's ratio of  $\varepsilon$ -FeOOH as a function of pressure. The solid red squares are longitudinal sound velocity ( $V_P$ ) measured using a reverse impact method under shock compression [12]; the solid blue squares and circles are  $V_P$  and shear sound velocity ( $V_S$ ) measured using an ultrasonic pulse-echo-overlap method at high pressures and 300 K [30]; the solid wine lines are bulk sound velocity ( $V_B$ ) of the high- and low-spin  $\varepsilon$ -FeOOH calculated using the Hugoniot equation of state in this paper; the wine dashed line is  $V_B$  of the mixed-spin (MS)  $\varepsilon$ -FeOOH estimated using the Hugoniot data in the spin crossover region; the open red circles are the  $V_S$  calculated based on a combination of our determined  $V_B$  and the  $V_P$  from Ref. [12]; the open green triangles, blue inverted triangles, and orange diamonds are adiabatic bulk modulus ( $K_S$ ), shear modulus ( $\mu$ ), and Poisson's ratio ( $\nu$ ) obtained in this paper, respectively; the solid gray line represents the  $V_P$  of seismic observations from the preliminary reference Earth model (PREM) [87]; the light-shaded area (47–61 GPa) is the spin crossover region with the MS state; all dotted dashed lines are guides to the eye. The uncertainties in the  $V_S$ ,  $K_S$ ,  $\mu$ , and  $\nu$  are estimated from the errors in  $\rho_H$ ,  $V_P$ , and  $V_B$  by using error propagation.

$\varepsilon$ -FeOOH remains a nearly constant of  $\sim 0.18$  in the regions of both HS and LS states; however, it is depressed to a negative value of  $-0.11$  at  $\sim 51$  GPa in the spin crossover region. This means that the spin transition of  $\text{Fe}^{3+}$  in  $\varepsilon$ -FeOOH results in

an abnormal auxeticity, and such a similar phenomenon has also been found in the  $\alpha$ - $\beta$  structural transition of quartz [92], the  $\beta$ - $\gamma$  structural transition of indium-tin (In-Sn) alloys [93], the cubic-tetragonal structural transition of barium titanate ( $\text{BaTiO}_3$ ) [94], and the HS-LS transition of magnesiosiderite [89]. The Landau theory of phase transitions indicates that elastic anomalies will occur upon approaching the phase boundary [95], leading to remarkable structural instability. Consequently, a phase transition is usually accompanied by a dramatic increase in compressibility, resulting in the softening of Poisson's ratio where it decreases to a negative value in the case of the spin transition of  $\text{Fe}^{3+}$  in  $\varepsilon$ - $\text{FeOOH}$ .

#### D. Effects of hydroxyl groups and temperature on the spin transition of $\text{Fe}^{3+}$

The present results of  $\varepsilon$ - $\text{FeOOH}$  also provide insight into the general spin-transition behavior and elastic wave-velocity anomalies of complex  $\text{Fe}^{3+}$ -bearing compounds that commonly exist in the lower mantle.  $\text{Fe}$ -bearing bridgmanite is the dominant mineral ( $\sim 75\%$  in volume) in Earth's lower mantle, which contains both  $\text{Fe}^{2+}$  and  $\text{Fe}^{3+}$ , whereas  $\text{Fe}^{3+}$  may appear in both dodecahedral A and octahedral B sites [1]. Recent experiments suggested that, if  $\text{Fe}^{3+}$  occupies the B site of bridgmanite, it will undergo the HS-LS transition at  $\sim 35$ – $45$  GPa and 300 K with a  $\sim 10$ – $15$  GPa pressure interval of HS-LS mixing state [11,21,65]. Meanwhile,  $\text{Fe}^{2+}$  and  $\text{Fe}^{3+}$  in the A site of bridgmanite remain in the HS state up to a pressure of the core-mantle boundary ( $\sim 136$  GPa) [3,21–23,96,97]. Similar spin-transition behavior is observed in the  $\text{Fe}$ -bearing NAL phase, which remains stable at high  $P$ - $T$  conditions relevant to the lower mantle [72,98,99]. Experimental studies showed that  $\text{Fe}^{3+}$  in the octahedral site of the NAL phase underwent the HS-LS transition at  $\sim 30$ – $40$  GPa and 300 K with a  $\sim 15$  GPa spin crossover pressure interval, but  $\text{Fe}^{3+}$  and  $\text{Fe}^{2+}$  in the trigonal-prismatic site remained in the HS state at least up to 80 GPa [72,100]. In short, only  $\text{Fe}^{3+}$  in the octahedral site undergoes the HS-LS transition in these phases. We should note that the spin transition of  $\text{Fe}^{3+}$  in bridgmanite and the NAL phase with lower  $\text{Fe}^{3+}$  content ( $\sim 10$ – $15$  GPa) is much more sluggish than that of  $\varepsilon$ - $\text{FeOOH}$  ( $\sim 2$  GPa) at 300 K, which may stem from the hydroxyl groups in  $\varepsilon$ - $\text{FeOOH}$ . The symmetrization of hydrogen bonds was reported to drive the spin transition of  $\text{Fe}^{3+}$  in  $\varepsilon$ - $\text{FeOOH}$  [13], while based on the measured lattice parameter ratios [5] and sound velocity at lower pressures ( $< 24$  GPa) [30], the hydrogen-bond symmetrization occurred at a lower pressure of  $\sim 18$  GPa and was unlikely to drive the spin transition of  $\text{Fe}^{3+}$  [5], but it may accelerate the spin transition by creating a close energy state that is more favorable for compressing the  $\text{FeO}_6$  octahedral chains [13].

It is known that applying high temperatures in  $\text{Fe}$ -bearing systems with spin transitions can provide higher vibrational entropy (and/or magnetic entropy) and configuration entropy to stabilize the HS and MS states, respectively. High  $P$ - $T$  theoretical calculation predicted a temperature derivative of  $\sim 7$  MPa/K of the spin transition of ferric ions in bridgmanite at high pressure by using density functional perturbation theory augmented by Hubbard type correction [101], which is in good agreement with our observation in  $\varepsilon$ - $\text{Fe}^{3+}\text{OOH}$

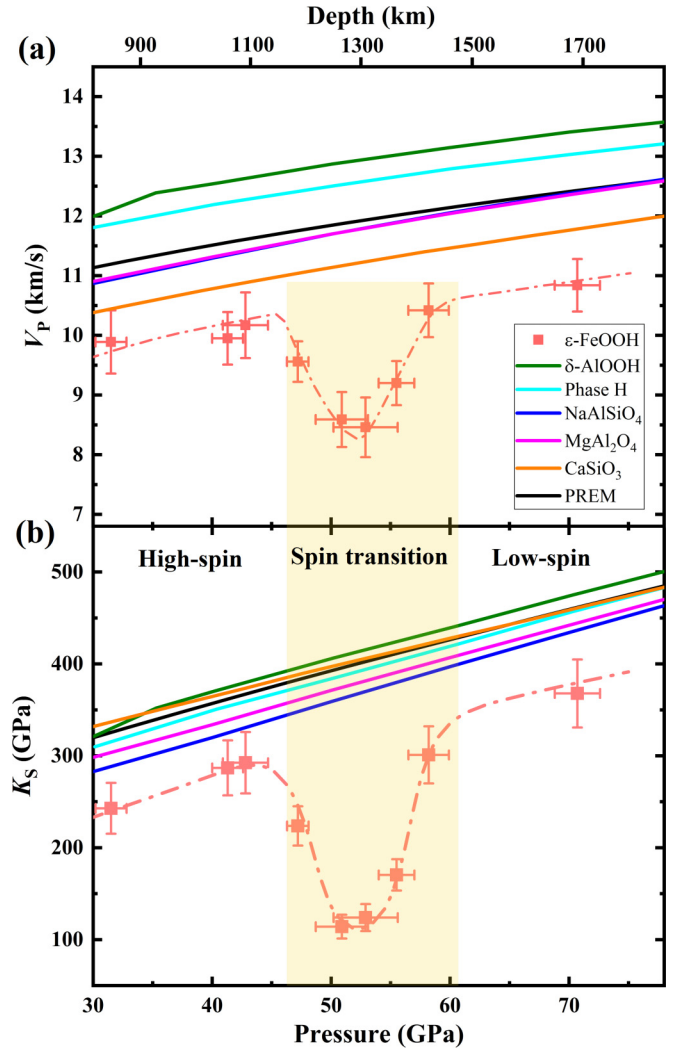


FIG. 5. Comparisons of (a) longitudinal sound velocity and (b) adiabatic bulk modulus between typical hydrous phases and other lower-mantle minerals at the conditions relevant to the lower mantle. Data sources:  $\varepsilon$ - $\text{FeOOH}$  (solid red squares), this study, and Ref. [12];  $\delta$ - $\text{AlOOH}$  (green curves), Ref. [104]; Phase H (cyan curves), Ref. [105];  $\text{NaAlSiO}_4$  (blue curves) and  $\text{MgAl}_2\text{O}_4$  (carmine curves), Ref. [107];  $\text{CaSiO}_3$  (orange curves), Ref. [106]; solid black curves are preliminary reference Earth model (PREM) values [87]. The dotted dashed lines are used to guide the eye, and the light-shaded area shows the spin crossover region of  $\text{Fe}^{3+}$  in  $\varepsilon$ - $\text{FeOOH}$ .

( $\sim 8$  MPa/K). The calculation [101] also showed that the broadening rate of the spin crossover range of  $\text{Fe}^{3+}$ -bearing bridgmanite is fast as  $\sim 20$  MPa/K, which is much larger than an earlier theoretical calculation of  $\sim 3.5$  MPa/K [102]. The difference between these two theoretical results may be related to the values of Hubbard  $U$  and the technique for vibrational density of states calculations [101]. Compared with  $\varepsilon$ - $\text{FeOOH}$ , the  $\text{Fe}^{3+}$ -bearing bridgmanite is absent of such hydroxyl groups, which is expected to have a faster broadening rate of spin crossover range. Thus, our results support the recent work [101], where the values of  $U$  were calculated self-consistently. We further estimate the spin transition of ferric



ions in Fe<sup>3+</sup>-bearing bridgmanite will occur between ~600 and ~1000 km on the basis of previous works [21,64,101].

### E. Spin transition of Fe<sup>3+</sup> in $\epsilon$ -FeOOH in Earth's lower mantle

As determined from our experiments and first-principles calculations (Fig. 3), the HS-LS transition of Fe<sup>3+</sup> in  $\epsilon$ -FeOOH spans over ~20 GPa at the  $P$ - $T$  conditions relevant to the subducting slabs, indicating the spin transition to continuously occur from a depth of 1400–1800 km of the lower mantle [83,84]. As FeOOH is abundant and widespread in sediments and ore deposits at the Earth's surface, it may form a solid solution with isostructural  $\delta$ -AlOOH and the phase H (MgSiO<sub>4</sub>H<sub>2</sub>) in the subducting slabs and remain thermodynamically stable down to the deep lower mantle [5,24–27,103]. The longitudinal sound velocity and adiabatic bulk modulus of  $\epsilon$ -FeOOH are lower than the average values of the preliminary reference Earth model (PREM) [87], those of  $\delta$ -AlOOH and the phase H [104,105], as well as some lower-mantle minerals, such as davemaoite (CaSiO<sub>3</sub>) [106], NaAlSiO<sub>4</sub>, and MgAl<sub>2</sub>O<sub>4</sub> [107], as shown in Fig. 5. Therefore, due to the spin crossover of Fe<sup>3+</sup> in  $\epsilon$ -FeOOH, the hydrous FeOOH-AlOOH-MgSiO<sub>4</sub>H<sub>2</sub> solid solutions are expected to exhibit abnormally low longitudinal sound velocity and adiabatic bulk modulus in the subducting slabs of the lower mantle, which may be detected as heterogeneities by seismology.

## IV. CONCLUSIONS

We have studied the spin-transition behavior and the thermoelastic properties of  $\epsilon$ -FeOOH through shock compression and first-principles simulation. The Hugoniot equation of state in FeOOH has been directly measured up to ~90 GPa and ~2100 K in a two-stage light-gas gun. The observed changes in the Hugoniot relations ( $U_s - u_p$  and  $P$ - $V$ ) identify a HS-to-

LS transition of Fe<sup>3+</sup> in  $\epsilon$ -FeOOH between 47 and 61 GPa along the Hugoniot pressure. The high  $P$ - $T$  phase diagram of  $\epsilon$ -FeOOH across its spin crossover was established by using first-principles calculations, which is in good agreement with our experiments. Combining the obtained Hugoniot equation of state with the previously measured longitudinal sound velocity, we further investigated the bulk and shear sound velocities, as well as the adiabatic bulk modulus, shear modulus, and Poisson's ratio of  $\epsilon$ -FeOOH at high  $P$ - $T$ . These results show that the spin transition in  $\epsilon$ -FeOOH softens the bulk sound velocity and adiabatic bulk modulus but slightly hardens the shear sound velocity and shear modulus. A negative Poisson's ratio of auxeticity is derived in the MS state.

Comparing the spin transition behavior of Fe<sup>3+</sup> in  $\epsilon$ -FeOOH with those in Fe<sup>3+</sup>-bearing bridgmanite and the NAL phase, we found that the hydroxyl groups (or hydrogen) have a profound effect on the spin transition of Fe<sup>3+</sup>, for example, accelerating the spin transition of Fe<sup>3+</sup>. The spin transition of Fe<sup>3+</sup> in  $\epsilon$ -FeOOH occurs in the lower mantle at a depth of 1400–1800 km along the geotherms of the subducting slabs, providing a possible source of seismic heterogeneities in the subducting slabs of the lower mantle.

### ACKNOWLEDGMENTS

The authors thank Xiaohong Li, Xilong Dou, Feng Gao, Yukai Zhuang, Qiming Wang, Shangchun Shi, and Yuanyuan Li for their help in shock-wave experiments. The authors thank Jian Song and three anonymous referees for their constructive comments that improved this paper. This paper was supported by the National Natural Science Foundation of China (No. 42074098, No. 11974253, and No. 42150101), the National Key R&D Program of China (No. 2017YFA0303600), and the Science Speciality Program of Sichuan University (No. 2020SCUNL210). Y.Z. acknowledges the support from the Sichuan Science and Technology Program (No. 2023NSFSC1910) and the Institutional Research Fund from Sichuan University (No. 2022SCUNL102).

- [1] J.-F. Lin, S. Speziale, Z. Mao, and H. Marquardt, Effects of the electronic spin transitions of iron in lower mantle minerals: Implications for deep mantle geophysics and geochemistry, *Rev. Geophys.* **51**, 244 (2013).
- [2] W. F. McDonough, Compositional model for the Earth's core, in *Treatise on Geochemistry*, 2nd ed., edited by H. D. Holland and K. K. Turekian (Elsevier, Oxford, 2014), p. 559.
- [3] J.-F. Lin, Z. Mao, J. Yang, J. Liu, Y. Xiao, P. Chow, and T. Okuchi, High-spin Fe<sup>2+</sup> and Fe<sup>3+</sup> in single-crystal aluminous bridgmanite in the lower mantle, *Geophys. Res. Lett.* **43**, 6952 (2016).
- [4] J.-F. Lin, V. V. Struzhkin, S. D. Jacobsen, M. Y. Hu, P. Chow, J. Kung, H. Liu, H.-K. Mao, and R. J. Hemley, Spin transition of iron in magnesiowüstite in the Earth's lower mantle, *Nature (London)* **436**, 377 (2005).
- [5] E. C. Thompson, A. H. Davis, N. M. Brauser, Z. Liu, V. B. Prakapenka, and A. J. Campbell, Phase transitions in  $\epsilon$ -FeOOH at high pressure and ambient temperature, *Am. Mineral.* **105**, 1769 (2020).
- [6] J. Badro, J.-P. Rueff, G. Vankó, G. Monaco, G. Fiquet, and F. Guyot, Electronic transitions in perovskite: Possible non-convecting layers in the lower mantle, *Science* **305**, 383 (2004).
- [7] J. Badro, G. Fiquet, F. Guyot, J.-P. Rueff, V. Struzhkin Viktor, G. Vankó, and G. Monaco, Iron partitioning in Earth's mantle: Toward a deep lower mantle discontinuity, *Science* **300**, 789 (2003).
- [8] E. Holmström and L. Stixrude, Spin Crossover in Ferropericlase from First-Principles Molecular Dynamics, *Phys. Rev. Lett.* **114**, 117202 (2015).
- [9] T. Tsuchiya, R. M. Wentzcovitch, C. R. S. da Silva, and S. de Gironcoli, Spin Transition in Magnesiowüstite in Earth's Lower Mantle, *Phys. Rev. Lett.* **96**, 198501 (2006).
- [10] M. W. Ammann, J. P. Brodholt, and D. P. Dobson, Ferrous iron diffusion in ferro-periclase across the spin transition, *Earth Planet. Sci. Lett.* **302**, 393 (2011).
- [11] S. Fu, J. Yang, Y. Zhang, T. Okuchi, C. McCammon, H.-I. Kim, S. K. Lee, and J.-F. Lin, Abnormal elasticity of Fe-bearing bridgmanite in the Earth's lower mantle, *Geophys. Res. Lett.* **45**, 4725 (2018).
- [12] Y. Zhuang, B. Gan, Z. Cui, R. Tang, R. Tao, M. Hou, G. Jiang, C. Popescu, G. Garbarino, Y. Zhang *et al.*, Mid-mantle water

- transportation implied by the electrical and seismic properties of  $\varepsilon$ -FeOOH, *Sci. Bull.* **67**, 748 (2022).
- [13] A. E. Gleason, C. E. Quiroga, A. Suzuki, R. Pentcheva, and W. L. Mao, Symmetrization driven spin transition in  $\varepsilon$ -FeOOH at high pressure, *Earth Planet. Sci. Lett.* **379**, 49 (2013).
- [14] G. Farfan, S. Wang, H. Ma, R. Caracas, and W. L. Mao, Bonding and structural changes in siderite at high pressure, *Am. Mineral.* **97**, 1421 (2012).
- [15] B. Chen, J. M. Jackson, W. Sturhahn, D. Zhang, J. Zhao, J. K. Wicks, and C. A. Murphy, Spin crossover equation of state and sound velocities of  $(\text{Mg}_{0.65}\text{Fe}_{0.35})\text{O}$  ferropericlyase to 140 GPa, *J. Geophys. Res.* **117**, B08208 (2012).
- [16] F. Goncharov Alexander, V. Struzhkin Viktor, and D. Jacobsen Steven, Reduced radiative conductivity of low-spin  $(\text{Mg,Fe})\text{O}$  in the lower mantle, *Science* **312**, 1205 (2006).
- [17] W.-P. Hsieh, T. Ishii, K.-H. Chao, J. Tsuchiya, F. Deschamps, and E. Ohtani, Spin transition of iron in  $\delta$ -(Al,Fe)OOH induces thermal anomalies in Earth's lower mantle, *Geophys. Res. Lett.* **47**, e2020GL087036 (2020).
- [18] A.-L. Auzende, J. Badro, F. J. Ryerson, P. K. Weber, S. J. Fallon, A. Addad, J. Siebert, and G. Fiquet, Element partitioning between magnesium silicate perovskite and ferropericlyase: New insights into bulk lower-mantle geochemistry, *Earth Planet. Sci. Lett.* **269**, 164 (2008).
- [19] H. Marquardt, S. Speziale, H. J. Reichmann, D. J. Frost, and F. R. Schilling, Single-crystal elasticity of  $(\text{Mg}_{0.9}\text{Fe}_{0.1})\text{O}$  to 81 GPa, *Earth Planet. Sci. Lett.* **287**, 345 (2009).
- [20] J. C. Crowhurst, J. M. Brown, A. F. Goncharov, and S. D. Jacobsen, Elasticity of  $(\text{Mg,Fe})\text{O}$  through the spin transition of iron in the lower mantle, *Science* **319**, 451 (2008).
- [21] K. Catalli, S.-H. Shim, V. B. Prakapenka, J. Zhao, W. Sturhahn, P. Chow, Y. Xiao, H. Liu, H. Cynn, and W. J. Evans, Spin state of ferric iron in  $\text{MgSiO}_3$  perovskite and its effect on elastic properties, *Earth Planet. Sci. Lett.* **289**, 68 (2010).
- [22] H. Hsu, P. Blaha, M. Cococcioni, and R. M. Wentzcovitch, Spin-State Crossover and Hyperfine Interactions of Ferric Iron in  $\text{MgSiO}_3$  Perovskite, *Phys. Rev. Lett.* **106**, 118501 (2011).
- [23] S. M. Dorfman, J. Badro, J.-P. Rueff, P. Chow, Y. Xiao, and P. Gillet, Composition dependence of spin transition in  $(\text{Mg, Fe})\text{SiO}_3$  bridgmanite, *Am. Mineral.* **100**, 2246 (2015).
- [24] B. Gan, Y. Zhang, Y. Huang, X. Li, Q. Wang, J. Li, Y. Zhuang, Y. Liu, and G. Jiang, Partial deoxygenation and dehydration of ferric oxyhydroxide in Earth's subducting slabs, *Geophys. Res. Lett.* **48**, e2021GL094446 (2021).
- [25] M. Nishi, Y. Kuwayama, J. Tsuchiya, and T. Tsuchiya, The pyrite-type high-pressure form of FeOOH, *Nature (London)* **547**, 205 (2017).
- [26] Q. Hu, D. Y. Kim, J. Liu, Y. Meng, L. Yang, D. Zhang, W. L. Mao, and H.-K. Mao, Dehydrogenation of goethite in Earth's deep lower mantle, *Proc. Natl Acad. Sci. USA* **114**, 1498 (2017).
- [27] Q. Hu, D. Y. Kim, W. Yang, L. Yang, Y. Meng, L. Zhang, and H.-K. Mao,  $\text{FeO}_2$  and FeOOH under deep lower-mantle conditions and Earth's oxygen-hydrogen cycles, *Nature (London)* **534**, 241 (2016).
- [28] E. Koemets, T. Fedotenko, S. Khandarkhaeva, M. Bykov, E. Bykova, M. Thielmann, S. Chariton, G. Aprilis, I. Koemets, K. Glazyrin *et al.*, Chemical stability of FeOOH at high pressure and temperature, and oxygen recycling in early Earth history, *Eur. J. Inorg. Chem.* **2021**, 3048 (2021).
- [29] T. Yoshino, E. Baker, and K. Duffey, Fate of water in subducted hydrous sediments deduced from stability fields of FeOOH and AlOOH up to 20 GPa, *Phys. Earth Planet. Inter.* **294**, 106295 (2019).
- [30] O. Ikeda, T. Sakamaki, T. Ohashi, M. Goto, Y. Higo, and A. Suzuki, Sound velocity measurements of  $\varepsilon$ -FeOOH up to 24 GPa, *J. Mineral. Petrol. Sci.* **114**, 155 (2019).
- [31] W. Xu, E. Greenberg, G. K. Rozenberg, M. P. Pasternak, E. Bykova, T. Boffa-Ballaran, L. Dubrovinsky, V. Prakapenka, M. Hanfland, O. Y. Vekilova *et al.*, Pressure-Induced Hydrogen Bond Symmetrization in Iron Oxyhydroxide, *Phys. Rev. Lett.* **111**, 175501 (2013).
- [32] K. Otte, R. Pentcheva, W. W. Schmahl, and J. R. Rustad, Pressure-induced structural and electronic transitions in FeOOH from first principles, *Phys. Rev. B* **80**, 205116 (2009).
- [33] D. Tunega, Theoretical study of properties of goethite ( $\alpha$ -FeOOH) at ambient and high-pressure conditions, *J. Phys. Chem. C* **116**, 6703 (2012).
- [34] M. M. Reagan, A. E. Gleason, L. Daemen, Y. Xiao, and W. L. Mao, High-pressure behavior of the polymorphs of FeOOH, *Am. Mineral.* **101**, 1483 (2016).
- [35] See Supplemental Material at <http://link.aps.org/supplemental/10.1103/PhysRevB.107.064106> for details of the experimental setup and theoretical simulations, analyses of the thermal stability, and elastic anomalies of  $\varepsilon$ -FeOOH at high pressure-temperature.
- [36] A. C. Mitchell and W. J. Nellis, Shock compression of aluminum, copper, and tantalum, *J. Appl. Phys.* **52**, 3363 (1981).
- [37] R. G. Kraus, J. P. Davis, C. T. Seagle, D. E. Fratanduono, D. C. Swift, J. L. Brown, and J. H. Eggert, Dynamic compression of copper to over 450 GPa: A high-pressure standard, *Phys. Rev. B* **93**, 134105 (2016).
- [38] J. M. Brown, J. N. Fritz, and R. S. Hixson, Hugoniot data for iron, *J. Appl. Phys.* **88**, 5496 (2000).
- [39] Q. Liu, X. Zhou, X. Zeng, and S. N. Luo, Sound velocity, equation of state, temperature and melting of LiF single crystals under shock compression, *J. Appl. Phys.* **117**, 045901 (2015).
- [40] G. Kresse and J. Furthmüller, Efficient iterative schemes for *ab initio* total-energy calculations using a plane-wave basis set, *Phys. Rev. B* **54**, 11169 (1996).
- [41] J. P. Perdew, K. Burke, and M. Ernzerhof, Generalized Gradient Approximation Made Simple, *Phys. Rev. Lett.* **77**, 3865 (1996).
- [42] R. M. Wentzcovitch, J. F. Justo, Z. Wu, C. R. S. da Silva, D. A. Yuen, and D. Kohlstedt, Anomalous compressibility of ferropericlyase throughout the iron spin cross-over, *Proc. Natl Acad. Sci. USA* **106**, 8447 (2009).
- [43] B. G. Jang, J. Liu, Q. Hu, K. Haule, H.-K. Mao, W. L. Mao, D. Y. Kim, and J. H. Shim, Electronic spin transition in  $\text{FeO}_2$ : Evidence for Fe(II) with peroxide  $\text{FeO}_2$ , *Phys. Rev. B* **100**, 014418 (2019).
- [44] S.-C. Zhu, Q. Hu, W. L. Mao, H.-K. Mao, and H. Sheng, Hydrogen-bond symmetrization breakdown and dehydrogenation mechanism of  $\text{FeO}_2\text{H}$  at high pressure, *J. Am. Chem. Soc.* **139**, 12129 (2017).
- [45] A. Togo and I. Tanaka, First principles phonon calculations in materials science, *Scr. Mater.* **108**, 1 (2015).
- [46] Z. Wu, J. F. Justo, and R. M. Wentzcovitch, Elastic Anomalies in a Spin-Crossover System: Ferropericlyase at Lower Mantle Conditions, *Phys. Rev. Lett.* **110**, 228501 (2013).

- [47] J. M. R. Muir and J. P. Brodholt, Ferrous iron partitioning in the lower mantle, *Phys. Earth Planet. Inter.* **257**, 12 (2016).
- [48] S. Root, J. P. Townsend, E. Davies, R. W. Lemke, D. E. Bliss, D. E. Fratanduono, R. G. Kraus, M. Millot, D. K. Spaulding, L. Shulenburg *et al.*, The principal Hugoniot of forsterite to 950 GPa, *Geophys. Res. Lett.* **45**, 3865 (2018).
- [49] B. L. Sherman, H. F. Wilson, D. Weeraratne, and B. Militzer, *Ab initio* simulations of hot dense methane during shock experiments, *Phys. Rev. B* **86**, 224113 (2012).
- [50] J. D. Kress, S. Mazevet, L. A. Collins, and W. W. Wood, Density-functional calculation of the Hugoniot of shocked liquid nitrogen, *Phys. Rev. B* **63**, 024203 (2000).
- [51] D. Li, P. Zhang, and J. Yan, Quantum molecular dynamics simulations for the nonmetal-metal transition in shocked methane, *Phys. Rev. B* **84**, 184204 (2011).
- [52] A. E. Gleason, R. Jeanloz, and M. Kunz, Pressure-temperature stability studies of FeOOH using x-ray diffraction, *Am. Mineral.* **93**, 1882 (2008).
- [53] F. Wiethoff, K.-D. Grevel, B. Marler, J. Herrmann, J. Majzlan, J. Kirste, and C. Lathe, *P-V-T* behavior of FeO(OH) and MnO(OH), *Phys. Chem. Miner.* **44**, 567 (2017).
- [54] R. Voigt and G. Will, Das System Fe<sub>2</sub>O<sub>3</sub>-H<sub>2</sub>O unter hohen Drücken (The system Fe<sub>2</sub>O<sub>3</sub>-H<sub>2</sub>O under high pressures), *Neues Jahrb. Mineral, Monatsh.* **2**, 89 (1981).
- [55] A. Suzuki, High-pressure x-ray diffraction study of  $\epsilon$ -FeOOH, *Phys. Chem. Miner.* **37**, 153 (2010).
- [56] A. Suzuki, Pressure-volume-temperature equation of state of  $\epsilon$ -FeOOH to 11 GPa and 700 K, *J. Mineral. Petrol. Sci.* **111**, 420 (2016).
- [57] S. P. Marsh, *LASL Shock Hugoniot Data* (University of California Press, Berkeley, 1980).
- [58] S. Wang, W. L. Mao, A. P. Sorini, C.-C. Chen, T. P. Devereaux, Y. Ding, Y. Xiao, P. Chow, N. Hiraoka, H. Ishii *et al.*, High-pressure evolution of Fe<sub>2</sub>O<sub>3</sub> electronic structure revealed by x-ray absorption, *Phys. Rev. B* **82**, 144428 (2010).
- [59] J. Kuneš, D. M. Korotin, M. A. Korotin, V. I. Anisimov, and P. Werner, Pressure-Driven Metal-Insulator Transition in Hematite from Dynamical Mean-Field Theory, *Phys. Rev. Lett.* **102**, 146402 (2009).
- [60] J. Badro, G. Fiquet, V. V. Struzhkin, M. Somayazulu, H.-k. Mao, G. Shen, and T. Le Bihan, Nature of the High-Pressure Transition in Fe<sub>2</sub>O<sub>3</sub> Hematite, *Phys. Rev. Lett.* **89**, 205504 (2002).
- [61] A. Sanson, I. Kantor, V. Cerantola, T. Irifune, A. Carnera, and S. Pascarelli, Local structure and spin transition in Fe<sub>2</sub>O<sub>3</sub> hematite at high pressure, *Phys. Rev. B* **94**, 014112 (2016).
- [62] Z. Mao, J.-F. Lin, J. Liu, and V. B. Prakapenka, Thermal equation of state of lower-mantle ferropericlase across the spin crossover, *Geophys. Res. Lett.* **38**, L23308 (2011).
- [63] Z. Mao, F. Wang, J.-F. Lin, S. Fu, J. Yang, X. Wu, T. Okuchi, N. Tomioka, V. B. Prakapenka, Y. Xiao *et al.*, Equation of state and hyperfine parameters of high-spin bridgmanite in the Earth's lower mantle by synchrotron x-ray diffraction and Mössbauer spectroscopy, *Am. Mineral.* **102**, 357 (2017).
- [64] Z. Mao, J.-F. Lin, J. Yang, T. Inoue, and V. B. Prakapenka, Effects of the Fe<sup>3+</sup> spin transition on the equation of state of bridgmanite, *Geophys. Res. Lett.* **42**, 4335 (2015).
- [65] J. Liu, S. M. Dorfman, F. Zhu, J. Li, Y. Wang, D. Zhang, Y. Xiao, W. Bi, and E. E. Alp, Valence and spin states of iron are invisible in Earth's lower mantle, *Nat. Commun.* **9**, 1284 (2018).
- [66] J. Liu, J.-F. Lin, Z. Mao, and V. B. Prakapenka, Thermal equation of state and spin transition of magnesiosiderite at high pressure and temperature, *Am. Mineral.* **99**, 84 (2014).
- [67] A. Mattila, T. Pylkkänen, J. P. Rueff, S. Huotari, G. Vankó, M. Hanfland, M. Lehtinen, and K. Hämäläinen, Pressure induced magnetic transition in siderite FeCO<sub>3</sub> studied by x-ray emission spectroscopy, *J. Phys.: Condens. Matter* **19**, 386206 (2007).
- [68] H. Shi, W. Luo, B. Johansson, and R. Ahuja, First-principles calculations of the electronic structure and pressure-induced magnetic transition in siderite FeCO<sub>3</sub>, *Phys. Rev. B* **78**, 155119 (2008).
- [69] B. Lavina, P. Dera, R. T. Downs, V. Prakapenka, M. Rivers, S. Sutton, and M. Nicol, Siderite at lower mantle conditions and the effects of the pressure-induced spin-pairing transition, *Geophys. Res. Lett.* **36**, L23306 (2009).
- [70] B. Lavina, P. Dera, R. T. Downs, W. Yang, S. Sinogeikin, Y. Meng, G. Shen, and D. Schiferl, Structure of siderite FeCO<sub>3</sub> to 56 GPa and hysteresis of its spin-pairing transition, *Phys. Rev. B* **82**, 064110 (2010).
- [71] T. Nagai, T. Ishido, Y. Seto, D. Nishio-Hamane, N. Sata, and K. Fujino, Pressure-induced spin transition in FeCO<sub>3</sub>-siderite studied by x-ray diffraction measurements, *J. Phys. Conf. Ser.* **215**, 012002 (2010).
- [72] Y. Wu, X. Wu, J.-F. Lin, C. A. McCammon, Y. Xiao, P. Chow, V. B. Prakapenka, T. Yoshino, S. Zhai, and S. Qin, Spin transition of ferric iron in the NAL phase: Implications for the seismic heterogeneities of subducted slabs in the lower mantle, *Earth Planet. Sci. Lett.* **434**, 91 (2016).
- [73] G. E. Duvall and R. A. Graham, Phase transitions under shock-wave loading, *Rev. Mod. Phys.* **49**, 523 (1977).
- [74] L. V. Al'tshuler, Phase transitions in shock waves (review), *J. Appl. Mech. Tech. Phys.* **19**, 496 (1978).
- [75] L. M. Barker and R. E. Hollenbach, Shock wave study of the  $\alpha \rightleftharpoons \epsilon$  phase transition in iron, *J. Appl. Phys.* **45**, 4872 (1974).
- [76] D. R. Curran, On the possibility of detecting shock-induced second-order phase transitions in solids. The equation of state of invar, *J. Appl. Phys.* **32**, 1811 (1961).
- [77] W. Sturhahn, J. M. Jackson, and J.-F. Lin, The spin state of iron in minerals of Earth's lower mantle, *Geophys. Res. Lett.* **32**, L12307 (2005).
- [78] J.-F. Lin, G. Vankó, D. Jacobsen Steven, V. Iota, V. Struzhkin Viktor, B. Prakapenka Vitali, A. Kuznetsov, and C.-S. Yoo, Spin transition zone in Earth's lower mantle, *Science* **317**, 1740 (2007).
- [79] T. Komabayashi, K. Hirose, Y. Nagaya, E. Sugimura, and Y. Ohishi, High-temperature compression of ferropericlase and the effect of temperature on iron spin transition, *Earth Planet. Sci. Lett.* **297**, 691 (2010).
- [80] Z. Wu, J. F. Justo, C. R. S. da Silva, S. de Gironcoli, and R. M. Wentzcovitch, Anomalous thermodynamic properties in ferropericlase throughout its spin crossover, *Phys. Rev. B* **80**, 014409 (2009).
- [81] R. G. McQueen, S. P. Marsh, J. W. Taylor, J. N. Fritz, and W. J. Carter, The equation of state of solids from shock wave studies, in *High-Velocity Impact Phenomena*, edited by R. Kinslow (Academic Press, San Diego, 1970), p. 293.

- [82] J. Majzlan, B. E. Lang, R. Stevens, A. Navrotsky, B. F. Woodfield, and J. Boerio-Goates, Thermodynamics of Fe oxides: Part I. Entropy at standard temperature and pressure and heat capacity of goethite ( $\alpha$ -FeOOH), lepidocrocite ( $\gamma$ -FeOOH), and maghemite ( $\gamma$ -Fe<sub>2</sub>O<sub>3</sub>), *Am. Mineral.* **88**, 846 (2003).
- [83] T. Katsura, A. Yoneda, D. Yamazaki, T. Yoshino, and E. Ito, Adiabatic temperature profile in the mantle, *Phys. Earth Planet. Inter.* **183**, 212 (2010).
- [84] F. Maeda, E. Ohtani, S. Kamada, T. Sakamaki, N. Hirao, and Y. Ohishi, Diamond formation in the deep lower mantle: A high-pressure reaction of MgCO<sub>3</sub> and SiO<sub>2</sub>, *Sci. Rep.* **7**, 40602 (2017).
- [85] B. G. Burns, *Mineralogical Applications of Crystal Field Theory* (Cambridge University Press, London, 1993).
- [86] J.-F. Lin, S. D. Jacobsen, W. Sturhahn, J. M. Jackson, J. Zhao, and C.-S. Yoo, Sound velocities of ferropiclasite in the Earth's lower mantle, *Geophys. Res. Lett.* **33**, L22304 (2006).
- [87] A. M. Dziewonski and D. L. Anderson, Preliminary reference Earth model, *Phys. Earth Planet. Inter.* **25**, 297 (1981).
- [88] H. Marquardt and A. R. Thomson, Experimental elasticity of Earth's deep mantle, *Nat. Rev. Earth Environ.* **1**, 455 (2020).
- [89] S. Fu, J. Yang, and J.-F. Lin, Abnormal Elasticity of Single-Crystal Magnesiosiderite Across the Spin Transition in Earth's Lower Mantle, *Phys. Rev. Lett.* **118**, 036402 (2017).
- [90] Y. Zhuang, L. Dai, L. Wu, H. Li, H. Hu, K. Liu, L. Yang, and C. Pu, Pressure-induced permanent metallization with reversible structural transition in molybdenum disulfide, *Appl. Phys. Lett.* **110**, 122103 (2017).
- [91] G. N. Greaves, A. L. Greer, R. S. Lakes, and T. Rouxel, Poisson's ratio and modern materials, *Nat. Mater.* **10**, 823 (2011).
- [92] R. E. A. McKnight, T. Moxon, A. Buckley, P. A. Taylor, T. W. Darling, and M. A. Carpenter, Grain size dependence of elastic anomalies accompanying the  $\alpha$ - $\beta$  phase transition in polycrystalline quartz, *J. Phys.: Condens. Matter* **20**, 075229 (2008).
- [93] D. Li, T. Jaglinski, D. S. Stone, and R. S. Lakes, Temperature insensitive negative Poisson's ratios in isotropic alloys near a morphotropic phase boundary, *Appl. Phys. Lett.* **101**, 251903 (2012).
- [94] L. Dong, D. S. Stone, and R. S. Lakes, Softening of bulk modulus and negative Poisson ratio in barium titanate ceramic near the Curie point, *Philos. Mag. Lett.* **90**, 23 (2010).
- [95] L. Landau, The theory of phase transitions, *Nature (London)* **138**, 840 (1936).
- [96] H. Hsu, K. Umamoto, P. Blaha, and R. M. Wentzcovitch, Spin states and hyperfine interactions of iron in (Mg, Fe)SiO<sub>3</sub> perovskite under pressure, *Earth Planet. Sci. Lett.* **294**, 19 (2010).
- [97] C. E. Mohn and R. G. Trønnes, Iron spin state and site distribution in FeAlO<sub>3</sub>-bearing bridgmanite, *Earth Planet. Sci. Lett.* **440**, 178 (2016).
- [98] A. Ricolleau, J.-P. Perrillat, G. Fiquet, I. Daniel, J. Matas, A. Addad, N. Menguy, H. Cardon, M. Mezouar, and N. Guignot, Phase relations and equation of state of a natural MORB: Implications for the density profile of subducted oceanic crust in the Earth's lower mantle, *J. Geophys. Res.* **115**, B08202 (2010).
- [99] T. Ishii, N. Miyajima, G. Criniti, Q. Hu, K. Glazyrin, and T. Katsura, High pressure-temperature phase relations of basaltic crust up to mid-mantle conditions, *Earth Planet. Sci. Lett.* **584**, 117472 (2022).
- [100] H. Hsu, First-principles study of iron spin crossover in the new hexagonal aluminous phase, *Phys. Rev. B* **95**, 020406(R) (2017).
- [101] G. Shukla, M. Cococcioni, and R. M. Wentzcovitch, Thermoelectricity of Fe<sup>3+</sup>- and Al-bearing bridgmanite: Effects of iron spin crossover, *Geophys. Res. Lett.* **43**, 5661 (2016).
- [102] T. Tsuchiya and X. Wang, Ab initio investigation on the high-temperature thermodynamic properties of Fe<sup>3+</sup>-bearing MgSiO<sub>3</sub> perovskite, *J. Geophys. Res.-Solid Earth* **118**, 83 (2013).
- [103] C. Xu, M. Nishi, and T. Inoue, Solubility behavior of  $\delta$ -AlOOH and  $\epsilon$ -FeOOH at high pressures, *Am. Mineral.* **104**, 1416 (2019).
- [104] J. Tsuchiya and T. Tsuchiya, Elastic properties of  $\delta$ -AlOOH under pressure: First principles investigation, *Phys. Earth Planet. Inter.* **174**, 122 (2009).
- [105] J. Tsuchiya and M. Mookherjee, Crystal structure, equation of state and elasticity of phase H (MgSiO<sub>4</sub>H<sub>2</sub>) at Earth's lower mantle pressures, *Sci. Rep.* **5**, 15534 (2015).
- [106] A. R. Thomson, W. A. Crichton, J. P. Brodholt, I. G. Wood, N. C. Siersch, J. M. R. Muir, D. P. Dobson, and S. A. Hunt, Seismic velocities of CaSiO<sub>3</sub> perovskite can explain LLSVPs in Earth's lower mantle, *Nature (London)* **572**, 643 (2019).
- [107] W. Wang, Y. Xu, D. Sun, S. Ni, R. Wentzcovitch, and Z. Wu, Velocity and density characteristics of subducted oceanic crust and the origin of lower-mantle heterogeneities, *Nat. Commun.* **11**, 64 (2020).